Plasma-Enabled Growth of Single-Crystalline SiC/AlSiC Core–Shell Nanowires on Porous Alumina Templates

ARTICLE *in* CRYSTAL GROWTH & DESIGN · JUNE 2012

Impact Factor: 4.89 · DOI: 10.1021/cg300103a

7 AUTHORS, INCLUDING:

Jinghua Fang
The Commonwealth Scientific and Industrial …
31 PUBLICATIONS **80** CITATIONS
SEE PROFILE

Kostya Ostrikov
The Commonwealth Scientific and Industrial …
521 PUBLICATIONS **8,124** CITATIONS
SEE PROFILE

S. Rubanov
University of Melbourne
101 PUBLICATIONS **1,108** CITATIONS
SEE PROFILE

S. Prawer
University of Melbourne
408 PUBLICATIONS **8,049** CITATIONS
SEE PROFILE

CRYSTAL GROWTH & DESIGN

Article

pubs.acs.org/crystal

Plasma-Enabled Growth of Single-Crystalline SiC/AlSiC Core–Shell Nanowires on Porous Alumina Templates

Jinghua Fang,*[,†,‡] Igor Aharonovich,[§] Igor Levchenko,[‡,∥] Kostya (Ken) Ostrikov,[‡,∥] Paul G. Spizzirri,[†] Sergey Rubanov,[#] and Steven Prawer[†]

[†]School of Physics, University of Melbourne, Parkville, VIC 3010, Australia

[‡]Plasma Nanoscience Centre Australia (PNCA), CSIRO Materials Science and Engineering, P.O. Box 218, Lindfield, NSW 2070, Australia

[§]School of Engineering and Applied Science, Harvard University, Cambridge, Massachusetts 02138, United States

[∥]Plasma Nanoscience, School of Physics, The University of Sydney, Sydney, NSW 2006, Australia

[#]Bio21 Institute, University of Melbourne, Parkville, Victoria 3010, Australia

Supporting Information

ABSTRACT: We report the catalyst-free synthesis of the arrays of core–shell, ultrathin, size-uniform SiC/AlSiC nanowires on the top of a periodic anodic aluminum oxide template. The nanowires were grown using an environmentally friendly, silane-free process by exposing the silicon supported porous alumina template to CH_4 + H_2 plasmas. High-resolution scanning and transmission electron microscopy studies revealed that the nanowires have a single-crystalline core with a diameter of about 10 nm and a thin (1–2 nm) amorphous AlSiC shell. Because of their remarkable length, high aspect ratio, and very high surface area-to-volume ratio, these unique structures are promising for nanoelectronic and nanophotonic applications that require efficient electron emission, light scattering, etc. A mechanism for nanowire growth is proposed based upon the reduction of the alumina template to nanosized metallic aluminum droplets forming between nanopores. The subsequent incorporation of silicon and carbon atoms from the plasma leads to nucleation and growth from the top of the alumina template.

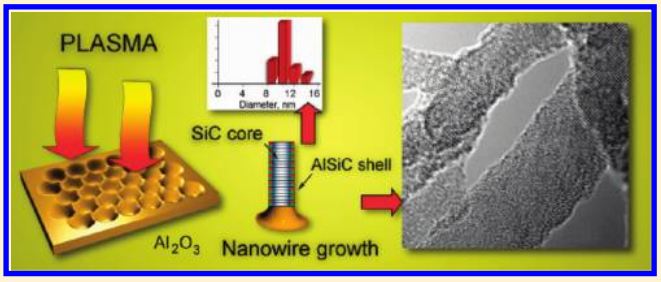

1. INTRODUCTION

Nanowires and other surface-based, one-dimensional nanostructures are very attractive for many advanced applications including nanoelectronics,[1] photonics,[2] plasmonics,[3] optoelectronics,[4] nanosensing,[5] and energy storage.[6] In contrast with bulk materials, one-dimensional nanostructures demonstrate many unique properties such as very long lengths and very high surface area-to-volume ratios, which may result in enhanced electroemissive properties, high catalytic activity, and improved heat transport. Among others, silicon carbide (SiC) is one of the most promising materials for the fabrication of nanowires since it has a wide electronic bandgap and superior mechanical, thermal, and chemical stability.[7,8] Implemented in nanoelectronic devices with applications in high power or high frequency operation, SiC could provide excellent thermal conductivity and high electric field strength properties ensuring efficient current multiplication.[9,10] Furthermore, crystalline SiC nanostructures show superior mechanical and field emission properties when compared to their bulk SiC counterparts,[11,12] and their recent use as negative-index metamaterials demonstrates the breadth of their application to novel areas.[13]

For one-dimensional nanostructured arrays to reach their full potential, one needs a simple, efficient, and environmentally friendly fabrication technique capable of producing size-uniform nanowires with the controlled structure. Nanowires have been successfully synthesized using a number of methods including decomposition of organic silicon compounds,[14] high-temperature reactions between carbon nanotubes and SiO,[15] arc-discharge processes,[16,17] hot filament chemical vapor deposition,[18] and low-temperature, atmospheric microplasma deposition.[19,20] These methods, however, have not been able to fabricate arrays of size-uniform SiC nanowires with precisely controlled internal structure. In addition, these techniques are very complex, slow, and harmful due to the use of the highly toxic precursor silane. Moreover, these processes are mostly based on the use of metal catalysts such as gold,[21] nickel,[22] aluminum,[23,24] and metal oxide,[25] which are often undesirable in the final product due to degradation of the array properties and contamination with metals affecting electronic device performance.

Template-assisted synthesis is a new and elegant approach for achieving highly controllable growth of the arrays of various

Received: January 24, 2012
Revised: April 12, 2012
Published: April 23, 2012

nanostructured materials. Porous anodic aluminum oxide (AAO) membranes have already been used as templates to fabricate arrays of carbon nanotubes[26,27] and nanowires.[28,29] In this process, the dimensions and density of the nanowires can be controlled by changing the length, width, and separation of the template channels. Using AAO templates and the chemical vapor deposition (CVD) technique, ordered arrays of SiC nanowires were produced.[30] Nevertheless, the process (which was conducted in a graphite heating furnace) took a long time (total reaction time > 60 h), and more importantly, it used highly toxic precursors. Control over the nanowire size was also limited in this process by the pore size (approximately 30 nm) of the alumina template.

Thus, the use of prefabricated AAO templates is a promising step toward the fabrication of highly ordered nanowire arrays. However, the practical processes still remain complex and hazard-prone and also suffer from poor control. Plasma-based fabrication techniques have recently been the subject of renewed interest because of the many effective process controls[31] and increased growth kinetics observed using these approaches. They may also provide control over the minimum nanowire thickness and lead to faster nanowire nucleation using lower processing temperatures.[32]

In this article, we report on a novel method for growing arrays of long, core−shell silicon carbide nanowires by exposing highly periodic (hexagonally symmetrical), porous anodic aluminum oxide templates to a low-temperature CH_4 + H_2 plasma. Characterization using transmission electron microscopy (TEM), scanning electron microscopy (SEM), electron-dispersive X-ray spectroscopy (EDX), and atomic force microscopy (AFM) techniques have shown that these nanowires have a single-crystalline SiC core and a thin amorphous AlSiC shell. We also propose a plausible three-stage mechanism of nanowire growth based upon the observed morphology of the substrate and nanowires at the end of the growth process. Our environmentally friendly, silane-free process is simple and fast and does not involve any predeposited metal catalysts. This novel fabrication technique constitutes another interesting application of alumina templates to nanowire growth.

2. EXPERIMENTAL SECTION

2.1. Synthesis. All chemical reagents (including gases) were used as received. Alumina templates were fabricated on quartz substrates using a two-step process. Initially, a quartz substrate (15 mm × 10 mm, 1 mm thick) was cleaned (ultrasonicated) in acetone and ethanol for 5 and 10 min, respectively, and then dried under nitrogen gas. A thin layer (1 μm) of high-purity (99.999%) aluminum was deposited using physical vapor deposition techniques onto a prepared substrate after which an anodization process[33] was employed to fabricate the templates as has been previously reported. The porous templates were then treated in a microwave plasma-enhanced CVD (PECVD) reactor for 30 min under the following conditions: substrate temperature ≈ 800 °C; microwave power ≈ 1200 W; and gas supply rates of 3.5 and 494 sccm for H_2 and CH_4, respectively. No precursor sources of silicon were introduced during growth leading us to believe that Si atoms were extracted from the silica base of the sample by intense ion sputtering through the template nanopores.[34] A schematic of this process is shown in Figure 1.

2.2. Characterization. The size, morphology, crystalline structure, and chemical composition of the templates and nanowires were both characterized using an FEI Nova Nanolab 200 field emission scanning electron microscope (FE-SEM), an FEI Tecnai TF20 high-resolution transmission electron microscope (HRTEM) with energy-dispersive X-ray spectroscopy (EDX), a JEOL 2100F electron energy-loss spectrometer (EELS), and a JEOL JSTM-4200 atomic force microscope (AFM). To reveal the internal structure of the template, a focused ion beam was used to mill the sample. To prevent the damage to the structure during milling, thin layers of Au and Pt were deposited onto the template face.

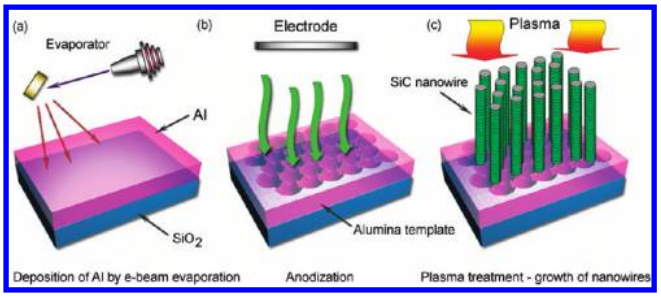

Figure 1. Schematic depiction of the SiC nanowire synthesis process. (a) Deposition of Al by e-beam evaporation on quartz; (b) AAO fabrication using an electrochemical cell; and (c) SiC nanowire growth on the top of AAO surface in the PECVD system.

3. RESULTS AND DISCUSSION

3.1. Morphological Features. Figure 2a shows a tilted plane view SEM image of the alumina template prior to the plasma-assisted nanowire growth. From this image, one can see that the nanopores in the template are uniform, ordered, and aligned in the vertical direction. A cross-sectional TEM image of the template is shown in Figure 2b where the thin black layers are the protective gold and platinum films. From this image, one can see that the walls between adjacent nanopores are very thin (not exceeding 30 nm) and become even thinner near the top surface of the template. Significantly, the nanopore walls appear to taper creating widened pore openings, thus forming an ordered array of sharp nanocones (i.e., periodic triangles in the cross-section).

In Figure 2c, an SEM image of the top surface of the template following nanowire growth is shown. We stress here that the nanowires were neither found on the side nor inside surfaces of the template; instead, the nanowires appeared to grow only on the top face of the template (i.e., on the surface that was in a direct contact with the plasma). A high-resolution TEM analysis has revealed a crystalline structure for these nanowires (Figure 2d).

In order to further characterize the ordering of the nanopores and the shape of the alumina walls at the top face of the template, we have used a high-resolution AFM for topographical analysis since this information may be critical for understanding the growth mechanism of the nanowires. As seen in Figure 2e, the openings of the nanopores are organized into a uniform hexagonal lattice with a gap between nanopore centers of approximately 60 nm. Moreover, the AFM analysis has confirmed that the walls between the nanopores taper off and form sharp nanocones.

To additionally confirm our assumption that the nanowires were nucleated and grown on the upper surface of the template (not inside the nanopores), we have partially removed the nanowires and then examined the obtained structure by SEM. One can clearly see that the nanopores are empty and that the nanowires do not originate on the walls inside the nanopores (Figure 2f). Thus, one can conclude that the ions from plasma do not reach the bottom through the holes in alumina. It is more likely that Si was supplied by sputtering of the clear Si surface at the margins around the alumina template, as well as at the substrate sides. This conclusion is also supported by our

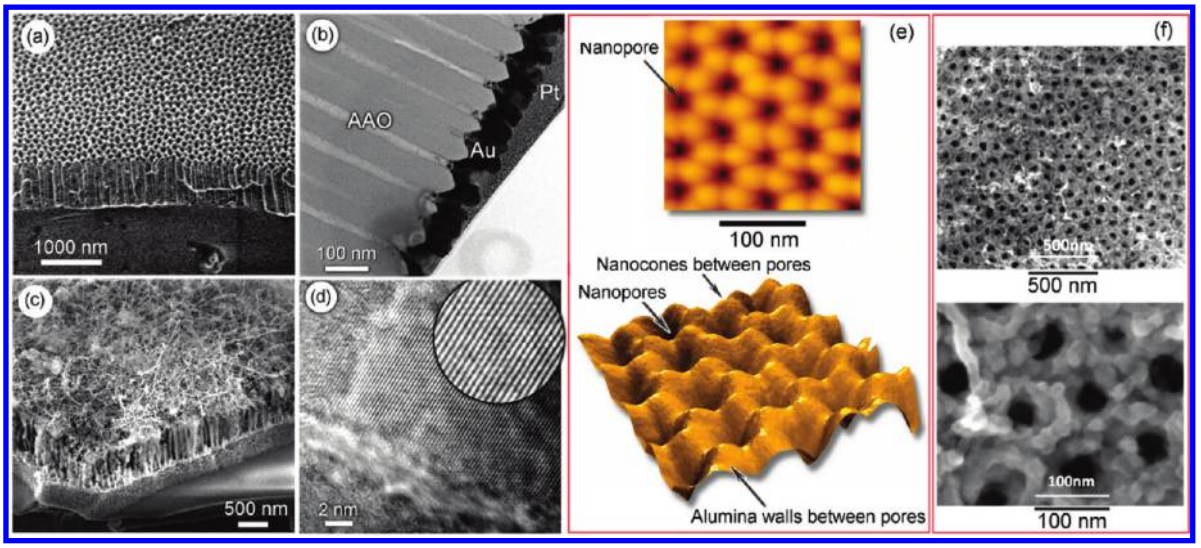

Figure 2. (a) Representative SEM image of the as-prepared alumina template on quartz. (b) FIB cut cross-section imaged using the TEM (the thin black layer is a gold coating followed by a platinum layer deposited to prevent damage to the template during the FIB milling). (c) SEM image of the template with nanowires on the top surface after the deposition in the PECVD reactor for 30 min. (d) HRTEM image of the nanowire, inset shows a crystalline structure. (e) High-resolution AFM image showing the hexagonal symmetry and ordering of the template surface before nanowire deposition. The lower panel shows the 3D morphology of the top surface of the template. (f) Low- and high-resolution SEM images of the alumina template surface after removal of most of the nanowires. It is seen that the nanopores are empty and that the nanowires do not nucleate on the walls inside the nanopores.

previous numerical simulations of ion transport in the narrow channels.[35]

3.2. Structural and Elemental Composition. Figure 3a shows a TEM image of the entangled net of the nanowires grown on the top surface of the porous alumina template. It can be seen that the length-to-radius ratio of the nanowires is quite large, reaching 100:1. The distribution of the nanowire diameters is rather narrow (see inset in Figure 3a). Figure 3b is a selected area electron diffraction pattern recorded from a bundle of nanowires showing individual diffraction spots indicative of a highly crystalline material. Clearly identifiable (111) and (220) atomic planes with the spacing of 0.251 and 0.153 nm, respectively, further support this statement. The circular arrangement of the diffraction spots, which has been accentuated in Figure 3b by red rings, originates (most likely) from measuring a multiwire bundle in which many orientations are probed simultaneously. TEM image of the 100 nm section of the nanowire shows a single-crystalline structure (Figure 3c).

EDX analysis was used to investigate the elemental composition and the internal structure of the nanowires in more detail. Figure 3d shows the EDX spectrum, which clearly indicates the presence of aluminum, carbon, and silicon (the copper signal originates from the TEM grid support). Moreover, the EDX line mapping shows that all the nanowires contain silicon, carbon, and aluminum as shown in Figure 3e.

3.3. Core–Shell Structure of the Nanowires. A high-resolution TEM image of a single nanowire is shown in Figure 4a. The image clearly shows that the perfectly crystalline nanowire core is encapsulated in an amorphous shell with a thickness of about 1 nm. A lattice interface spacing of 0.251 nm was measured from this data, which is consistent with the (111) lattice spacing of β-SiC. To reveal the chemical composition and distribution of elements across the nanowires, EELS analysis was performed. The plot in Figure 4b shows an EELS line scan recorded across the nanowire shown in Figure 4a (yellow trace). This analysis reveals that both silicon and carbon are present throughout the nanowire cross-section. The Si concentration peaks near the outer shell, while the concentration of carbon decreases. Furthermore, EELS analysis has shown that silicon and carbon have approximately equal concentrations in the crystalline core, thus forming near-stoichiometric SiC. In contrast, the concentration of aluminum is very low in the nanowire core; however, this metal is more prevalent in the shell. Note that the EELS results are consistent with the EDX measurements showing the presence of silicon, carbon, and aluminum. More TEM images of the nanowire structure are shown in the Supporting Information, Figure S1.

Figure 4c shows a Si L-loss spectrum recorded from the core of the nanowire. This spectrum is typical for Si in crystalline SiC.[36] Moreover, the carbon K-loss peak at (285 eV) is lower than 290 eV indicating that the carbon is sp^3-bonded, which is common for crystalline SiC.[37] Hence, the combination of HRTEM, EELS, and EDX analyses makes it possible to confidently conclude that the nanowires are composed of a crystalline SiC core and an amorphous AlSiC shell. Hereinafter, we will refer to this structure as SiC/AlSiC nanowires.

To confirm the crystalline structure of the fabricated nanowires, we have made an XRD characterization that has revealed the presence of several characteristic planes (Figure 5a). To study the variation in the chemical composition of the nanowire along its length, we have repeated cross-sectional EELS scans several times, changing the scan position relative to the nanowire tip (two typical scans illustrating the aluminum content are shown in Figure 5b). Numerical integration of these graphs has shown that the aluminum content decreases as 1:0.82:0.61 with the scan line position moving away from the nanowire tip, thus evidencing that the nanowire tip contains the maximum amount of aluminum.

3.4. Proposed Growth Mechanism. Our studies have revealed the following: (i) effective growth of the long nanowires occurs on alumina nanocones situated between the AAO nanopores in the absence of an intentionally introduced metal catalyst; (ii) SiC/AlSiC nanowires have a core–shell structure with a near-stoichiometric SiC core and an aluminum-

dx.doi.org/10.1021/cg300103a | Cryst. Growth Des. 2012, 12, 2917–2922

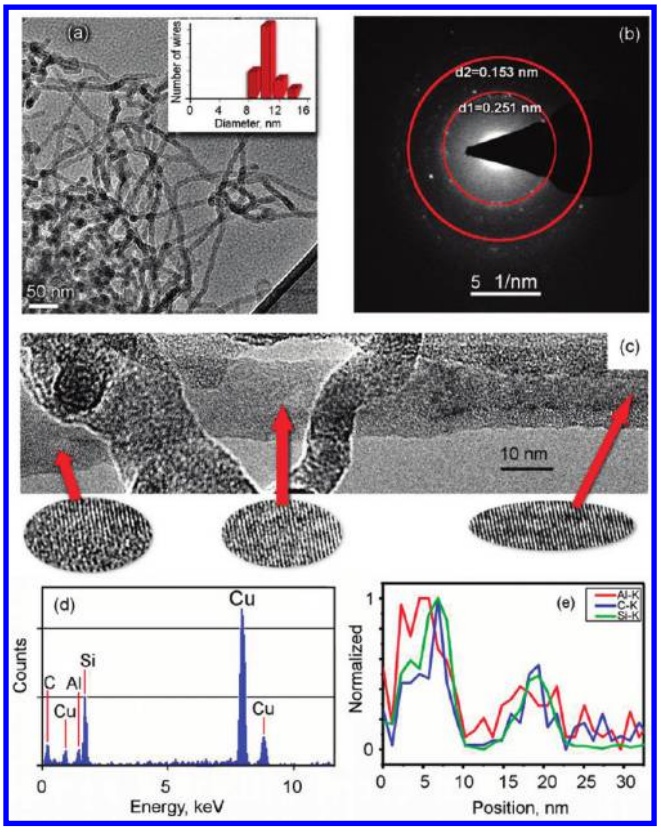

Figure 3. (a) TEM image of the entangled net of nanowires (the inset shows the distribution of the nanowire diameters). (b) Diffraction pattern recorded from the nanowire bundle. The first and the second rings correspond to (111) and (220) planes of β-SiC, respectively. (c) TEM image of a long nanowire section showing the single-crystalline structure. (d) EDX spectrum recorded from a bundle of nanowires showing the presence of Al, Si, C, and Cu elements. The signal from Cu originates from the supporting TEM grid, while the other elements are present in the nanowire. (e) EDX line mapping spectrum of the two nanowires, with the Si, C, and Al signals present.

enriched shell; and (iii) the nanowire core has a single-crystalline structure. To account for these observations, we will now propose a plausible growth mechanism, which is consistent with the above features of the nanowire growth.

First, let us identify the specific catalyst responsible for the nucleation and growth of the SiC nanowires on the AAO templates. In principle, Al_2O_3 can exhibit (like other oxides) a

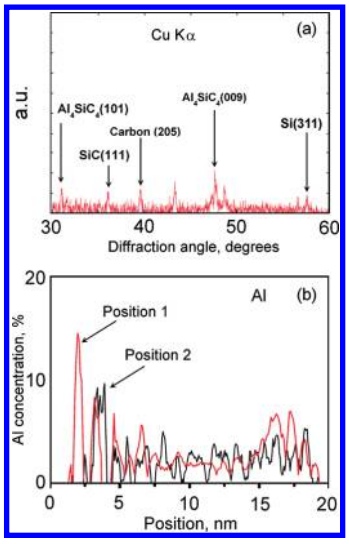

Figure 5. (a) XRD analysis of the fabricated sample. (b) Two cross-sectional EELS scans made at different distances from the nanowire tip, showing the change in aluminum content.

certain catalytic activity; however, this activity can be quite low due to its high stability and low reactivity. Indeed, a catalyst- and oxygen-free process conducted in a heating furnace has been reported, which resulted in the fabrication of pure (metal-free) SiC nanowires, most probably catalyzed by alumina. While this process was quite long (lasting up to several hours), it does provide some insight into the catalytic activity of alumina under the conditions similar to those of our work.[30] The process described in this work was faster (taking around 30 min) but still not as fast as the growth based on very active metal catalysts. Therefore, Al_2O_3 was not the primary catalyst in our process, and some other catalytic material with a higher catalytic activity was responsible for the nucleation and growth.

Silicon dioxide is another material that potentially could be responsible for catalyzing the wire growth. Indeed, there are reports of SiO_2 catalyzing the nucleation and growth of Si nanowires[38] and carbon nanostructures.[39] Nevertheless, such a mechanism is improbable under the conditions of our work since the reactive gas mixture did not contain free oxygen to form SiO_2. However, the conversion $Al_2O_3 \rightarrow SiO_2$ is not favorable due to a very large difference in the enthalpies of formation for Al_2O_3 and SiO_2 (which are -1675.7 and -910.9 kJ·mol^{-1}, respectively). In addition, no traces of oxygen were found in the nanowires.

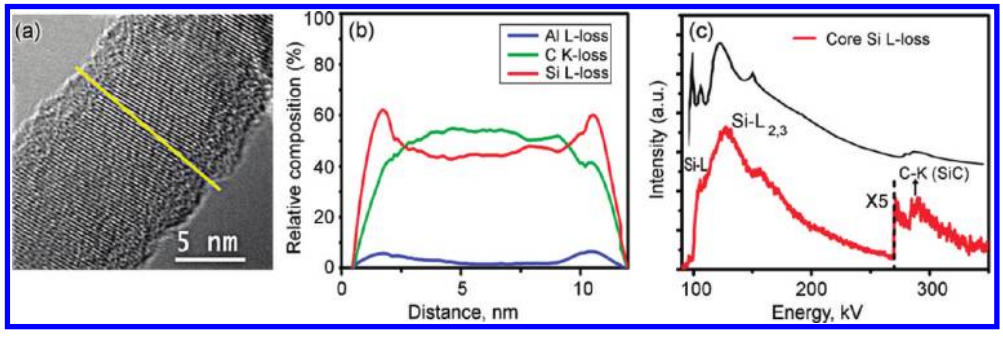

Figure 4. (a) HRTEM image of the nanowire, revealing the ⟨111⟩ crystal planes of β-SiC. A crystalline nanowire core is encapsulated in the amorphous shell with the thickness of about 1 nm. (b) An EELS line scan spectrum of the nanowire recorded along the yellow line shown in panel a. (c) Silicon electron energy L-loss spectra recorded from the core of the nanowire. A typical SiC EELS spectrum (black line) is shown above the spectra.

dx.doi.org/10.1021/cg300103a | Cryst. Growth Des. 2012, 12, 2917−2922

A third possibility is pure aluminum, which is also present in abundance in the nanowires and thus could be responsible for the catalysis. If this were the case, the vapor−liquid−solid (VLS)[40] mechanism could well be the main mechanism of nanowire growth. Indeed, the presence of residual metal in the nanowires is a common signature of the metal-assisted VLS mechanism. However, the availability of reduced (pure) aluminum at the nucleation and growth sites (on the tips of the alumina nanocones) requires an additional justification. Alumina is chemically a very stable compound; hence, reduction of alumina to a pure metal state at the process temperature used in this work (800 °C) is questionable, even in a strongly reducing (hydrogen-rich) environment. Indeed, it has been shown that alumina can be effectively reduced to Al in hydrogen atmosphere at temperatures exceeding 1000 °C.[41] Nevertheless, in our plasma-based process, the effective heating and activation of the alumina nanocones is possible due to strong ion bombardment of the nanocone tips[42] resulting in the formation of small (several nm) Al nanoparticles. Conversely, strong ion bombardment will also reduce the amount of Al due to sputtering and possible sublimation/evaporation effects.

To investigate the concept of plasma-reduced Al nanoparticle formation resulting in nanowire catalysis, we have prepared similar templates as free-standing (i.e., removed from the silicon substrate) scaffolds and performed nanowire growth under the same conditions. It is known that aluminum shows a weak catalytic activity toward carbon and usually cannot produce nanotubes. Indeed, while transition metals featuring a few d-vacancies exhibit the best ability for catalyzing growth of carbon-based nanostructures due to overlapping d-orbitals with p-orbitals of carbon atoms, aluminum is an element of s-type and, as such, is not very active toward carbon.[44] Nevertheless, other workers have demonstrated that, under similar conditions to this work, aluminum can catalyze the nucleation and growth of long carbon nanowires.[43] Thus, in our case, one might expect the formation of surface-supported carbon nanostructures on Al nanoparticles, as it was reported.[44] Nevertheless, we did not find any signs of carbon nanowires on the free-standing alumina templates (refer to the SEM image shown in Figure S2a of the Supporting Information). Additionally, another growth run using a sapphire substrate (unstructured) did not reveal any vertical nanostructures (refer to Figure S2b in the Supporting Information).

We conclude, therefore, that Al nanoparticles in the plasma environment (strong heating and sputtering) cannot survive for the time required to allow nanowire growth, and since the SiC nanowires did grow (i.e., catalysis is effective) when Si is present, one can assume that some metastable transitional phase involving Si and capable of converting into SiC is formed in the reaction zone.

Our proposed mechanism of formation of the SiC/AlSiC nanowires can be described as follows (see schematic of the process shown in Figure 6.) Ionized hydrogen and methane gases provide strong heating of the tips of the alumina nanocones resulting in its reduction to pure liquid aluminum, which is then carburized by the reaction $4Al + 3C \rightarrow Al_4C_3$. Aluminum carbide Al_4C_3 is a relatively unstable compound (compared with alumina) with a decomposition temperature around 1400 °C. This intermediate compound may then participate in the two-way reaction $Al_4C_3 + 3Si \leftrightarrow 4Al + 3SiC$ to form silicon carbide. This reaction is energetically unfavorable and can only proceed as a result of a very strong local heating in the plasma environment. Thus, the formation of aluminum carbide prevents the metallic Al from evaporating, keeping it in the metastable phase. Because of the multiphase nature of the SiC formation mechanism, it is synthesized mainly at the catalyst-nanowire interface thus forming an excellent crystal structure, as was observed in this work.

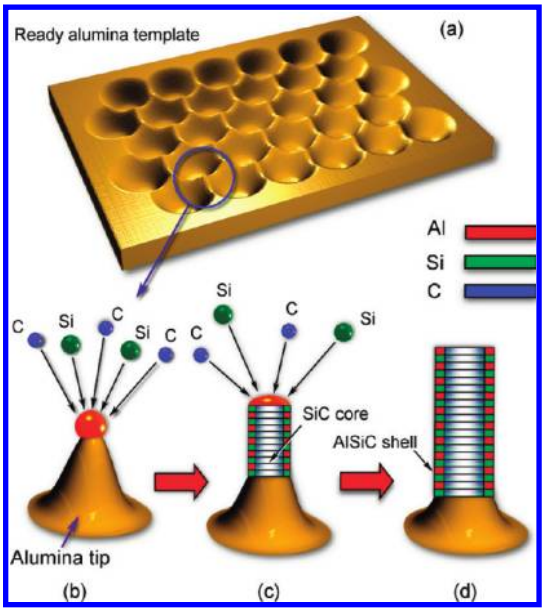

Figure 6. Schematic illustration of the proposed growth mechanism of the SiC/AlSiC core−shell nanowires. (a) A highly periodic alumina (AAO) template with a cone shaped, tapered tip geometry is fabricated. (b) During the CVD process, the high field points of the tapered tips are reduced and etched by hydrogen radicals resulting in the formation of an initial Al droplet. (c) Silicon atoms from the quartz substrate and carbon atoms from the methane gas source diffuse and participate in the reaction resulting in the nanowire nucleation. (d) The growth stops once the Al is etched by the plasma.

Pure aluminum released in the $Al_4C_3 \rightarrow SiC$ transformation diffuses into the silicon carbide matrix, forming a profile with a low concentration in the center of the nanowire and a higher concentration at the outer layers. It can be also noted that this profile is similar to the presumable shape of the temperature distribution across the fast-growing wall-heated nanowire. The heat transfer along the nanowire is quite effective,[45] and the growth rate in plasma is very high due to the intense ion and atom fluxes, as well as material diffusion along the nanowire. As a result, it can be expected that the growing upper part of the nanowire will have lower temperature in the core and higher temperature at the walls due to the intense electron heating of the nanowire walls.

Some decrease in the Al concentration in the outermost layers of the nanowire can be explained by Al evaporation from the hot nanowire surface. The thickness of the amorphous shell (of about 1 nm) is determined by the requirement to reduce the surface energy of the nanowire.[46,47]

3.5. Estimation of the Nanowire Diameter. Using the above-mentioned growth mechanism and the geometrical characteristics of the alumina template measured using the AFM and TEM techniques, we have estimated that the nanowire diameter is within the 10−15 nm range, which is in a good agreement with our experimental results (refer to the Supporting Material).

dx.doi.org/10.1021/cg300103a | Cryst. Growth Des. 2012, 12, 2917−2922

4. CONCLUSIONS

The growth of ultrathin (~10 nm diameter) core−shell SiC/AlSiC nanowires using a rapid and simple, single-step, silane-free, environmentally friendly method is reported. These nanowires were grown on the top of AAO templates, which were exposed to a $CH_4 + H_2$ plasma in a CVD reactor without any additional metallic catalyst. A three-stage growth mechanism is proposed, similar to that of the well-known VLS mechanism that involves (1) reduction of the alumina template to form metallic Al droplets; (2) incorporation of silicon and carbon atoms into the metallic droplet; and (3) precipitation and growth of the nanowire. This simple fabrication method results in the formation of uniformly sized, crystalline core−shell nanowires and constitutes another interesting application of alumina templates to nanowire growth.

■ ASSOCIATED CONTENT

Supporting Information

TEM images of the nanowires, SEM images of the free-standing template and sapphire surface after CVD process, and estimation of the nanowire radius. This material is available free of charge via the Internet at http://pubs.acs.org.

■ AUTHOR INFORMATION

Corresponding Author

*E-mail: Jinghua.Fang@csiro.au.

Notes

The authors declare no competing financial interest.

■ ACKNOWLEDGMENTS

This work was supported by the Australian Research Council (LP100100824 and DP1096288) and CSIRO's OCE Science Leadership Program. J.-H.F. acknowledges support by CSIRO's OCE Postdoctoral Fellowship Scheme. We would like to thank Dr A. Stacey for help with the CVD reactor and Dr D. Lau for the EELS measurements.

■ REFERENCES

(1) Yao, Y.; Lee, S. T.; Li, F. H. *Chem. Phys. Lett.* **2003**, *381*, 628−633.
(2) Li, H. J.; Li, Z. J.; Meng, A. L.; Li, K. Z.; Zhang, X. N.; Xu, Y. P. *J. Alloys Compd.* **2003**, *352*, 279−282.
(3) Akimov, Y. A.; Koh, W. S. *Nanotechnology* **2010**, *21*, 235201.
(4) Mariotti, D. *Appl. Phys. Lett.* **2008**, *92*, 151505.
(5) Mozetič, M.; Cvelbar, U.; Sunkara, M. K.; Vaddiraju, S. *Adv. Mater.* **2005**, *17*, 2138−2142.
(6) Liu, R.; Lee, S. B. *J. Am. Chem. Soc.* **2008**, *130*, 2942−2943.
(7) Hatty, V.; Kahn, H.; Trevino, J.; Zorman, C. A.; Mehregany, M.; Ballarini, R.; Heuer, A. H. *J. Appl. Phys.* **2006**, *99*, 013517.
(8) Yonenaga, I.; Hoshi, T.; Usui, A. *J. Phys.: Condens. Matter* **2000**, *12*, 10319.
(9) Ajayan, P. M.; Ebbesen, T. W.; Ichihashi, T.; Iijima, S.; Tanigaki, K.; Hiura, H. *Nature* **1993**, *362*, 522−525.
(10) Fissel, A.; Schroter, B.; Richter, W. *Appl. Phys. Lett.* **1995**, *66*, 3182−3184.
(11) Zhang, X. F.; Sixta, M. E.; De Jonghe, L. C. *J. Am. Ceram. Soc.* **2000**, *83*, 2813−2820.
(12) Wong, E. W.; Sheehan, P. E.; Lieber, C. M. *Science* **1997**, *277*, 1971−1975.
(13) Cai, W.; Chettiar, U. K.; Kildishev, A. V.; Shalaev, V. M. *Opt. Express* **2008**, *16*, 5444−5452.
(14) Addamiano, A. *J. Cryst. Growth* **1982**, *58*, 617−622.
(15) Zhou, D.; Seraphin, S. *Chem. Phys. Lett.* **1994**, *222*, 233−238.
(16) Volotskova, O.; Fagan, J. A.; Huh, J. Y.; Phelan, F. R.; Shashurin, A.; Keidar, M. *ACS Nano* **2010**, *4*, 5187−5192.
(17) Seeger, T.; Kohler-Redlich, P. *Adv. Mater.* **2000**, *12*, 279−282.
(18) Kamlag, Y.; Goossens, A.; Colbeck, I.; Schoonman, J. *Appl. Surf. Sci.* **2001**, *184*, 118−122.
(19) Mariotti, D.; Švrček, V.; Kim, D.-G. *Appl. Phys. Lett.* **2007**, *91*, 183111.
(20) Chiang, W.-H.; Sankaran, R. M. *Nat. Mater.* **2009**, *8*, 882−886.
(21) Ostrikov, K. *Rev. Mod. Phys.* **2005**, *77*, 489−511.
(22) Levchenko, I.; Ostrikov, K. *Nanotechnology* **2008**, *19*, 335703.
(23) Gao, F.; Yang, W.; Wang, H.; Fan, Y.; Xie, Z.; An, L. *Cryst. Growth Des.* **2008**, *8*, 1461−1464.
(24) Wang, Y.; Schmidt, V.; Senz, S.; Gösele, U. *Nat. Nanotechnol* **2006**, *1*, 186−189.
(25) Niu, J. J.; Wang, J. N. *J. Phys. Chem. B* **2007**, *111*, 4368−4373.
(26) Gao, H.; Mu, C.; Wang, F.; Xu, D.; Wu, K.; Xie, Y.; Liu, S.; Wang, E.; Xu, J.; Yu, D. *J. Appl. Phys.* **2003**, *93*, 5602−5605.
(27) Sui, Y. C.; Acosta, D. R.; Gonzalez-Leon, J. A.; Bermudez, A.; Feuchtwanger, J.; Cui, B. Z.; Flores, J. O.; Saniger, J. M. *J. Phys. Chem. B* **2001**, *105*, 1523−1527.
(28) Zong, R. L.; Zhou, J.; Li, B.; Fu, M.; Shi, S. K.; Li, L. T. *J. Chem. Phys.* **2005**, *123*, 094710.
(29) Liu, C. H.; Yiu, W. C.; Au, F. C. K.; Ding, J. X.; Lee, C. S.; Lee, S. T. *Appl. Phys. Lett.* **2009**, *83*, 3168−3170.
(30) Li, Z.; Zhang, J.; Meng, A.; Guo, J. *J. Phys. Chem. B* **2006**, *110*, 22382−22386.
(31) Ostrikov, K.; Cvelbar, U.; Murphy, A. B. *J. Phys. D: Appl. Phys.* **2011**, *44*, 174001.
(32) Ostrikov, K.; Seo, D. H.; Mehdipour, H.; Cheng, Q.; Kumar, S. *Nanoscale* **2012**, *4*, 1497−1508.
(33) Fang, J. H.; Spizzirri, P.; Cimmino, A.; Rubanov, S.; Prawer, S. *Nanotechnology* **2009**, *20*, 065706.
(34) Xu, S.; Levchenko, I.; Huang, S. Y.; Ostrikov, K. *Appl. Phys. Lett.* **2009**, *95*, 111505.
(35) Yuan, L.; Zhong, X.; Levchenko, I.; Xia, Y.; Ostrikov, K. *Plasma Processes Polym.* **2007**, *4*, 612−620.
(36) Yu, D. P.; Xing, Y. J.; Tence, M.; Pan, H. Y.; Leprince-Wang, Y. *Phys. E* **2002**, *15*, 1−5.
(37) Goel, S.; Luo, X.; Reuben, R. L.; Rashid, W. B. *Nanoscale Res. Lett.* **2011**, *6*, 589−598.
(38) Zhang, R. Q.; Lifshitz, Y.; Lee, S. T. *Adv. Mater.* **2003**, *15*, 635−640.
(39) Liu, B.; Ren, W.; Gao, L.; Li, S.; Pei, S.; Liu, C. *J. Am. Chem. Soc.* **2009**, *131*, 2082−2083.
(40) Fan, H. J.; Werner, P.; Zacharias, M. *Small* **2006**, *2*, 700−717.
(41) Braaten, O.; Kjekshus, A.; Kvande, H. *JOM* **2000**, *52*, 47−53.
(42) Levchenko, I.; Huang, S. Y.; Ostrikov, K.; Xu, S. *Nanotechnology* **2010**, *21*, 025605.
(43) Sung, C.-M.; Tai, M. F. *Int. J. Refract. Met. Hard Mater.* **1997**, *15*, 237−256.
(44) Esconjauregui, S.; Whelan, C. M.; Maex, K. *Carbon* **2009**, *47*, 659−669.
(45) Volklein, F.; Schmitt, M. C.; Reith, H.; Huzel, D. *Nanowires: Implementations and Applications*; InTech: Rijeka, Croatia, 2011.
(46) Lauhon, L. J.; Gudiksen, M. S.; Wang, D.; Lieber, C. M. *Nature* **2002**, *420*, 57−61.
(47) Zhang, H. F.; Wang, C. M.; Wang, L. S. *Nano Lett.* **2002**, *2*, 941−944.